Characterisation of low reflectivity antenna supports for electrically small antennas, and pattern measurement via optical fibre to eliminate common mode current errors

Martin Alexander, George Palikaras*, Andrea Sani*, Marie Rajab*

National Physical Laboratory, Teddington, UK
*Queen Mary University of London, UK

Abstract
Electrically small antennas are widely used in wireless communications applications because they have near omni-directional radiation. Development of wearable computer systems has been growing rapidly: electrically, as well as physically, small antennas are important requirements to the successful deployment in the consumer market [1]. It is undesirable to use bulky cables to connect to these wearable-mobile devices, so communication will be wireless, using an antenna. The biggest measurement challenge is to minimise reflections from antenna supports and feed cables. For reasons of space or cost small antennas may not have adequate baluns, and this can result in common mode currents flowing on any cable attached to them. These currents form an integral part of the antenna's radiation pattern.
One solution to avoid the problem with test cables is to replace the cable by optical fibre which connects to the antenna via an electro-optic transducer. A breakthrough reported in this paper is the development of a miniature electro-optic transducer. This system transfers the same information to a vector network analyser that a cable would but with the advantage that it can dramatically clean up the radiation pattern.

Introduction
When measuring antennas with omni-directional radiation patterns there is usually the issue of minimising measurement errors by reducing reflections from the environment, from the antenna support and from the antenna feeder cable. The term "omni-directional" is used loosely in this paper to cover antennas whose desirable property is to radiate in all directions, implying a poor backlobe to front ratio. The worst case is when the antenna gives rise to a greater portion of its input energy as common mode current on the feeder cable and when this nulls out the intended radiation from the antenna giving pattern errors of up to 15 dB. Most mobile antennas will not have a feed cable in their final application, but it may be useful to have a feed cable in the development of the antenna. It is also acknowledged that common mode current may not matter in the final application, because it is the radiation from the whole assembly, such as a mobile phone or a wearable on-body wireless sensor, that counts. However when designing an antenna, especially complex multiband ones with frequency notches, it is helpful to be able to see the performance of the antenna alone without being compromised by common mode radiation.

At frequencies below around 200 MHz common mode current can be attenuated to some extent by putting ferrite clamps on the cable but these are ineffective at higher frequencies. This problem is eliminated when the cable is replaced by optical-fibre. The amount of metal on the electro-optic transducer (here called OEFS) is little larger than twice the size of a SMA terminal panel plug, which is much smaller than other proprietary RF-optical links. The signal via the OEFS is the same as that via a coaxial cable, but there is approximately 30 dB loss which can be compensated by using an RF amplifier. However, this may not be necessary if the analyser has a low noise floor, as the OEFS has a dynamic range exceeding 100 dB.

Even if there is insignificant common mode current it is still desirable to eliminate radiation induced cable currents, especially where the cable is aligned with the antenna polarisation. For an

antenna with a good balun, and hence no common mode current, NPL has found that the cable can cause an error in antenna gain of up to 1 dB depending on the proximity of the cable to the antenna.

In April 2008, NPL commissioned an anechoic chamber specifically for the measurement of wireless communications antennas at frequencies of 400 MHz and above. This was coined the SMART chamber for Small Antenna Radiated Testing and to reflect that the purpose was also to measure smart antennas. The shielded room is 7 m long x 6.25 m high x 6.25 m wide and is lined with TDK polyethylene 45 cm high pyramidal absorber. This is more robust than the more common polyurethane absorber and can be covered with easily relocatable polystyrene walkover tiles. The absorber on the walls and ceiling is capped by thin polystyrene tiles, as shown in the photographs below, and a light in each corner of the ceiling gives excellent illumination aided by these tiles. The chamber is equipped with an Orbit Powercell roll-over-azimuth positioner, which has a Kevlar mast. This mast is designed to be both a low reflectivity structure and to be CTIA compliant. The mast is on a precision platform with a screw thread such that, by winding a handle, the antenna can be situated above the azimuth axis of rotation.

This paper reports on the performance of this chamber by measuring changes in the received signal of a dipole antenna that is resonant at 2.055 GHz. It focuses on the effects that are due to the Orbit mast, the antenna mount, the roll positioner and it's rotating mechanism..

For antennas with a cardioid radiation pattern, the influence of the roll mechanism (and entire mast) can be virtually eliminated by mounting the antenna with its null pointing in the direction of the roll mechanism, as explained below in relation to Fig. 4.

The roll mechanism comprises a belt made of Neopren reinforced with Kevlar fibres, and a number of other parts, shown in Photo D, which are made of POM, alternatively known as Delrin. This material has similar RF properties to PTFE but is more machinable. The paper includes the measured radiation pattern at 900 MHz of a PIFA antenna from a mobile phone, to demonstrate the enormous advantage of connection via optical-fibre to combat common mode radiation.

NPL worked in partnership with QMUL, whose staff were given access to this measurement facility, which also served NPL to hone the facility and measurement techniques for needed applications. The paper provides further evidence in support of the optical-fibre measurement set up compared to the coaxial cable counterpart with measured results on an ultra wideband (UWB) body-worn antenna as well as an implantable Radio Frequency Identification (RFID) antenna for body-centric wireless communications, operating at 3.1-10.6 GHz and 868MHz (UHF) bands respectively. The proposed UWB antenna is a physically small CPW-fed tapered slot antenna (TSA) [3] as shown in Fig. 9. Fig. 10 depicts the implantable RFID as a meandered PIFA antenna type [4] that is optimised to operate whilst embedded in an artificially fabricated 3-layer Phantom representative of skin, fat and muscle. These antennas were developed by the Body-Centric Wireless Sensor Lab (BodyWiSe) at Queen Mary, University of London. The key considerations when designing body-worn antennas are: the antenna itself must be small and lightweight, since it is part of a lightweight device; the small size of the antenna must not reduce its performance; the antenna structure must be designed to have limited radiation power in the direction of the wearer, to minimize possible health problems; and the transmission power must be low, to prolong battery life and hence operating time.

Measurements

The radiation pattern of a proprietary dipole antenna was measured in order to make comparisons of the results under various mounting conditions. The antenna was a European Antenna dipole model EVD2-1920-2175/548 with a frequency range of 1.92 GHz to 2.175 GHz. Radiation patterns were measured at 1.92, 2.055 and 2.175 GHz. Only the centre frequency is reported here because the

differences were similar at the ends of the band. This investigation relied on the availability of an antenna assumed to have a uniform H-plane pattern and further measurements are required to cover the desired UWB frequencies up to 11 GHz. The graphs below are of single pattern cuts with a 0.25 dB grid (unless otherwise stated) on the ordinate, and -180˚ to +180˚ in 20˚ steps on the abscissa. NPL had previously assessed the performance of the room by measuring the coupling between pairs of miniature biconical antennas up to 8 GHz [2]. It was found that the walkover blocks made excellent low reflective antenna supports, with less than 0.2 dB effect on the coupling. Photo A shows the antenna mounted on a block, though the best performance is with the antenna on the underside of the block as shown in Photo E, because the top has a layer of denser foam.

The initial aim was to achieve a radiation pattern of the dipole with negligible effect from the antenna support. Fig. 1 shows two attempts to minimise the influence of the antenna support on the radiation pattern. The dipole was taped to a foam bracket such that the radiating element was clear of the top of the mast, giving the red plot; this was an azimuth cut of the H-plane. Then the dipole was mounted with its null on the roll axis and the blue plot is a roll cut of the H-plane. Unfortunately the distances between the source horn and the dipole had not been carefully monitored and adjusted for the various configurations so the relative level of the plots is uncertain. However by eye one can see good agreement of the plots as a whole and it is estimated that the blue plot in Fig. 1 is 0.15 dB too high. This equates to a distance difference of 40 mm in 2.3 m. For this paper the red plot has been chosen as the reference plot. It shows a variation of ±0.35 dB over the H-plane cut. Fig. 1 shows that the plots agree to 0.5dB.

To further determine the uniformity of the H-plane pattern, the dipole (Photo E) was rotated about its axis by 180˚ and the measurement repeated. The two plots are compared in Fig. 2. If a single plot is the true dipole pattern, one would expect the features of the rotated dipole to be 180˚ away from the original. This is almost the case if one were to interpret the peak on the red plot at +100 to correspond with the dip on the blue plot at −100 ; there is obviously some influence of the mount on the pattern. The blue plot on Fig. 2 should correspond to the blue plot on Fig. 1 but the azimuth axis had been rotated through 180 . This is clarified by comparing the blue and purple (dashed) plots on Fig. 3. The reason for rotating Az from +90˚ to −90˚ was another opportunity to see to what extent the mast (and environment) was having on the pattern. In fact rotating Azimuth had almost negligible effect because the blue plot is almost identical to the reverse of the purple plot.

In conclusion it does seem that the dipole does not have a uniform pattern, but its pattern is consistent in three different ways of mounting the antenna to within 0.5 dB. Therefore in the antenna mounts aimed to minimise the effect of the mast (including the foam bracket), the mast is having an effect within ±0.25 dB. Fig. 4 shows the E-plane pattern when the antenna is mounted with its null facing the roll mechanism. There is good symmetry of the mainlobes and a sharp null 32 dB deep null, which further indicates negligible reflection from the mast and/or very little unwanted scatter from elsewhere, indicating good anechoic performance of the chamber.

Not all antennas have cardioid radiation patterns that enable the roll mechanism to be hidden in a null, and it may not be possible to mount the antenna with its null pointing to the mechanism. So further explorations were made of possible antenna mounts and the effects on the radiation patterns.

Fig. 5 shows the pattern of the antenna mounted on a foam block. There is generally agreement within 0.5 dB of the reference plots, with a maximum difference of 1 dB. The blue plot is actually with the antenna mounted on the bottom surface of the foam block, as shown in Photo E, which has less effect on an antenna as explained above.

Fig. 6 shows the patterns with the dipole taped to the side of the Kevlar tube in order to be clear of the roll mechanism, however there is still the belt inside the tube. For the blue plot the dipole was

taped to the front of the mast where it was facing the flat sides of the belt, and the purple (dashed) plot is where the dipole was moved around to the side of the mast (at the same height) where it was facing the two cross section sides of the belt. The spread of results is 1.6 dB which is worse than the best mounting setups reported above.

For Fig. 7 the dipole was mounted on the Orbit foam bracket, but this time vertically as shown in Photo F, rather than with its null pointing to the roll mechanism. Even though the separation from mechanism is ~0.5 m, the deviation from the reference plot in the forward direction +1/-1.2 dB, but this increases to +2/-2.5 dB when the azimuth angle is near 180 , i.e. with the mechanism intervening between the dipole and the source antenna. Fig. 7b is the polar format of 7a. In order to see the worst-case effect of the roll mechanism, the dipole was mounted close to it as shown in Photo D. The deviation from the reference plot was ±3 dB.

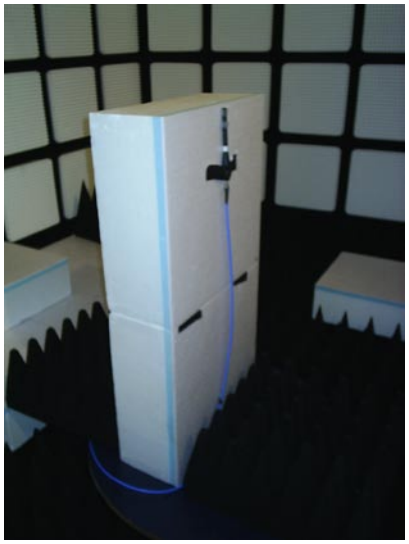

Photo A. Dipole on top surface of foam block (was also put on bottom surface, less density)

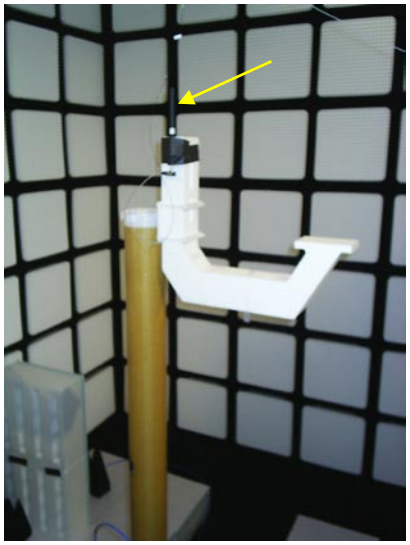

Photo B. Dipole raised clear of supports and connected to OEFS and optical fibre.

Photo C. Dipole on Kevlar tube, which enclosed plastic roll belt.

Photo D. Dipole near roll mechanism, worst case. Showing foam platform.

Photo E. Dipole with null facing roll mechanism. Shows bottom surface of foam blocks.

Photo F. Dipole on foam bracket for azimuth scan to give H-plane pattern.

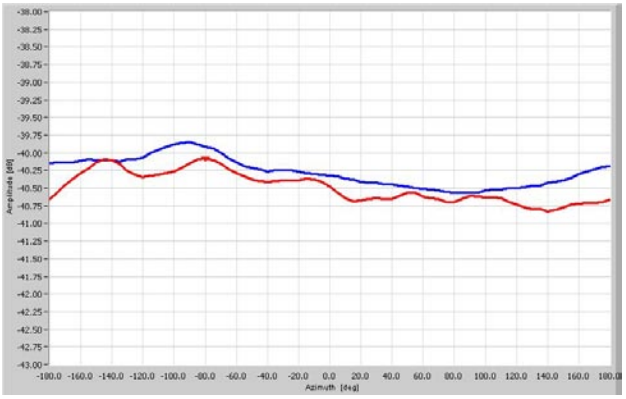

Figure 1. Red – reference plot, photo B. Blue - tip facing Tx horn, Roll cut, photo E.

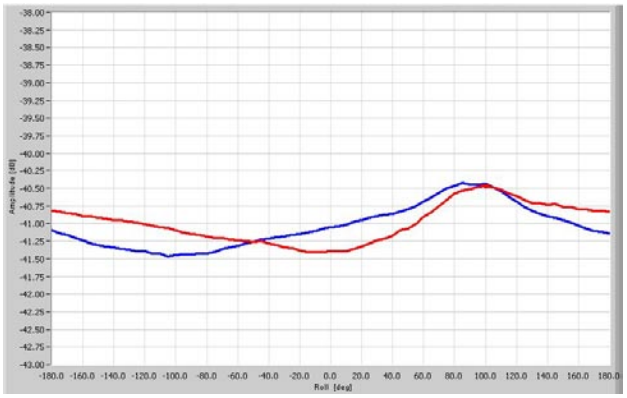

Figure 2. Dipole tip facing Tx horn, antenna rotated 180˚ to assess effect of foam platform, photo E (roll cut reverse of that in Fig. 1).

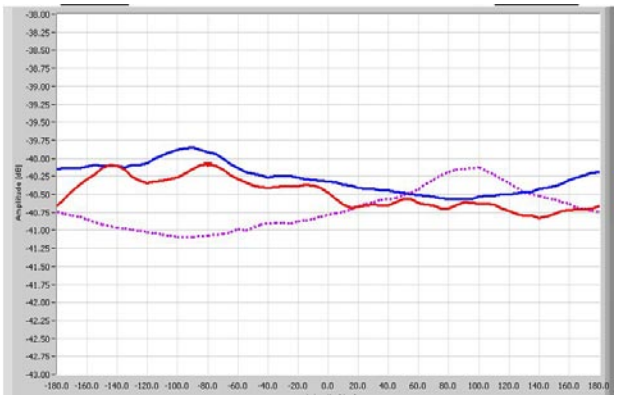

Figure 3. Dipole tip facing Tx horn, same roll cut with Az =+90˚ (blue) & Az=-90˚ (dashed). Red is reference plot

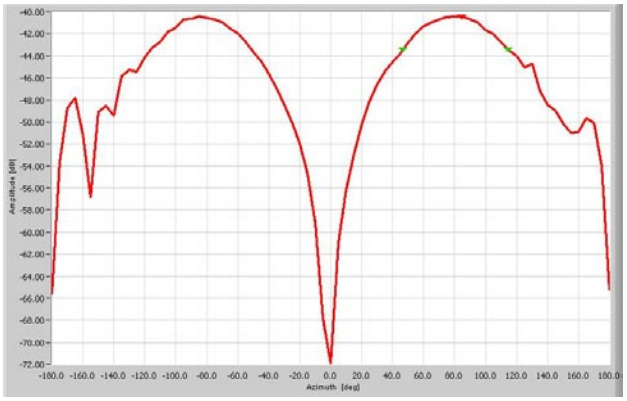

Figure 4. Dipole tip facing Tx horn, Az cut = E-plane, photo E but Roll rotated 90˚ for bracket as photo F. Y-axis scale 2 dB grid.

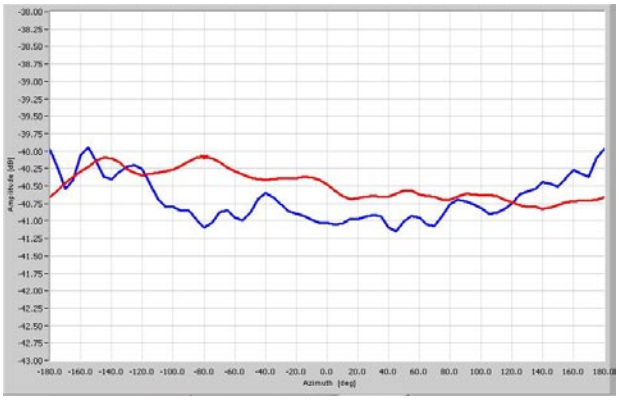

Figure 5. Red - reference plot, photo B. Blue - at top of 2 blocks of walkover, photo A.

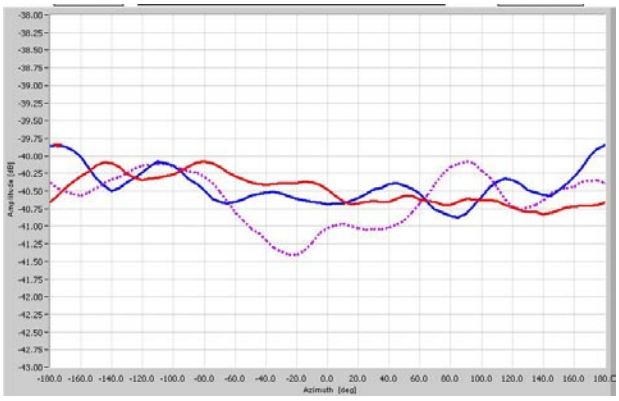

Figure 6. Red – reference plot, photo B. Blue - dipole on front of mast 30 cm below roll axis. Purple dipole on side of mast, photo C.

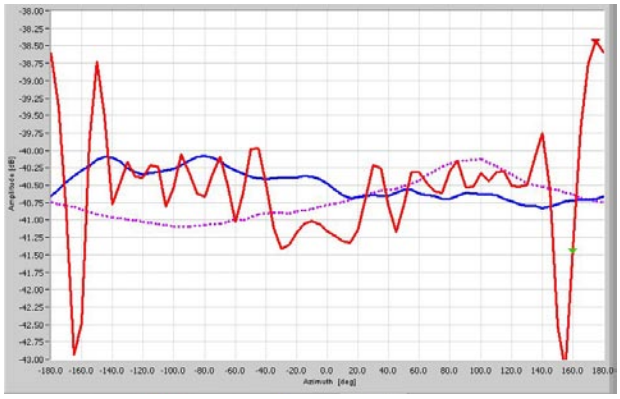

Figure 7a. Blue – reference plot, photo B. Red dipole vertical on foam bracket, photo F.

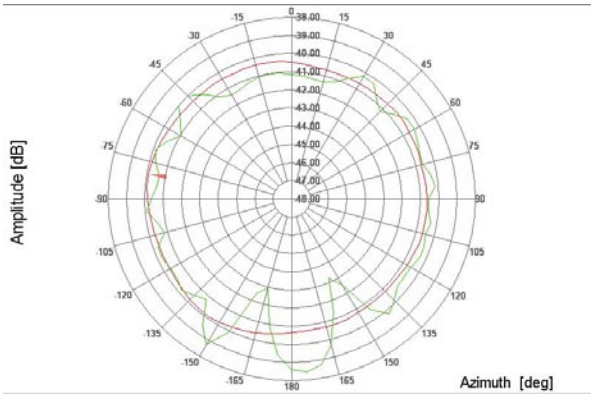

Figure 7b. As Fig. 7a but polar. Red – reference plot, photo B. Green - dipole on front of mast 30 cm below roll axis, photo F. Scale 1 dB per div.

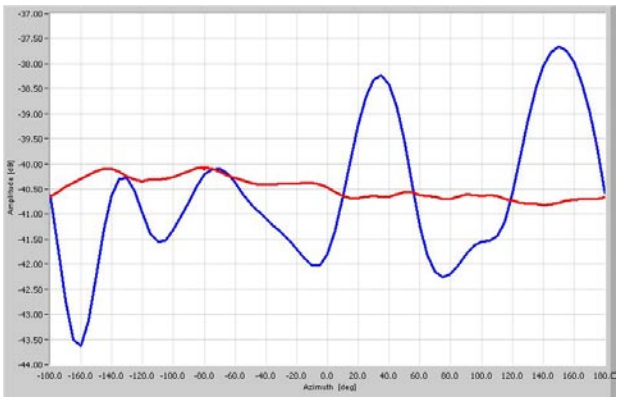

Figure 8. Red – reference plot, photo B. Blue at top of 2 blocks of walkover, photo D. Y-axis scale 0.5 dB grid.

RF-optical link (OEFS)

NPL started working with the NEC-Tokin Corporation of Japan in 2000 to improve the stability and usability of electro-optic sensors. The heart of these is a Mach-Zehnder interferometer on a lithium-niobate chip in which the RF signal is picked up by small electrodes which change the refractive index of one of a pair of waveguide channels in the chip, thereby modulating the 1550nm laser light. The response is sub-nanosecond and capable of transferring an RF signal up to at least 40 GHz. The actual OEFS system has currently reached 10 GHz, with a bottom frequency of 300 kHz. The dynamic range is at least 130 dB. The sensitivity to electromagnetic field depends on the size and shape of the electrodes or antenna. With a 100 mm long dipole the sensitivity is better than 0.1 mV/m. A three-axis sensor was developed within a 6 mm diameter head in the form of a field probe for SAR measurements in human simulants. The advantage of this over rival versions was that the complete signal was transferred rather than a rectified DC version. In 2006 the optical division was transferred to Seikoh-giken who continued development, in particular in the form of a transducer to enable a direct connection to any antenna. The key feature of this transducer is its small size, with the aim of minimising distortion of the antenna and invasiveness of the antenna field. Another advantage is the low loss through hundreds of metres of fibre compared with cable. A possible application is remote monitoring of fields. As an example NPL did some measurements for a railway network to measure fields associated with voltage spikes due to a build up of harmonics on the train's overhead electricity supply. These were causing sub-station failures. The use of optical fibre was an advantage over coaxial cable in the proximity of field strengths of kV/m/

Fig. 9 shows the OEFS controller that houses a pair of 10mW lasers which are orthogonally polarised in order that higher cost polarisation maintaining fibre does not have to be used. The sensors have mirrors and the retuned light enters a circulator and on to an RF detector diode. There is an RF amplifier to partially compensate for the loss of the RF signal. The 3 inputs are for a 3-axis sensor, but the transducer uses one input. There is feedback from the level of returned light to the RF amplifier to compensate for up to 1 dB change in RF level due to movement of the fibre.

Figure 9. PIFA antenna connected to Electro-optic transducer that is connected to the OEFS controller unit.

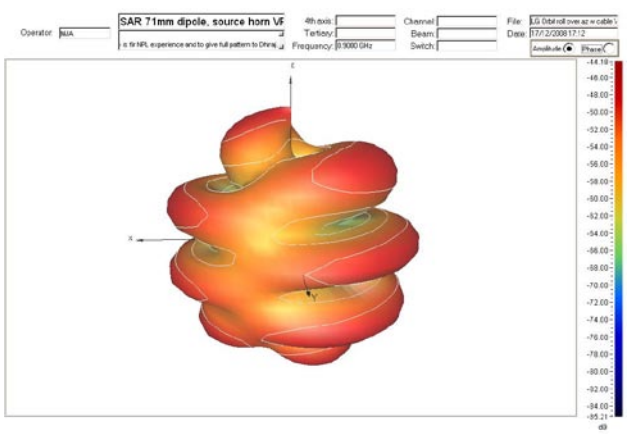

Figure 10a PIFA antenna with coaxial cable

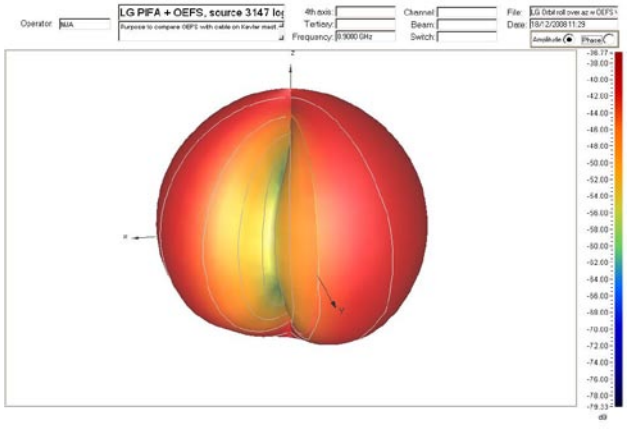

Figure 10b PIFA antenna with optical fibre

Fig. 10a shows the 3D pattern of a PIFA antenna at 900 MHz which is mounted on the platform on the Orbit foam bracket, is connected to a semi-rigid cable that goes straight back through the roll axis to a rotating joint. A coaxial cable connected to the other side of the joint is routed vertically down the back of the mast to another rotating joint on the azimuth axis.

Fig. 10b shows the 3D pattern of the same setup as for Fig. 10a, except that the coaxial cables are removed and the antenna is connected to the transducer in the way shown in Fig. 9.

The antenna is less than 50 mm in dimension, so at 900 MHz it is electrically small and a cardioid pattern is expected. The use of the OEFS gives a very nice cardioid pattern, compared to the deep nulls when using coax due to the interaction of the radiation mainly from the vertically hanging cable, destructively interfering with the antenna radiation as the assembly is rotated in azimuth

Measurement of body mounted and implantable antennas (QMUL)

The Orbit mast was removed and a 1 m diameter wooden turntable was screwed to the plate on top of the azimuth positioner. The measurements are explained below by the photos and graphs and captions.

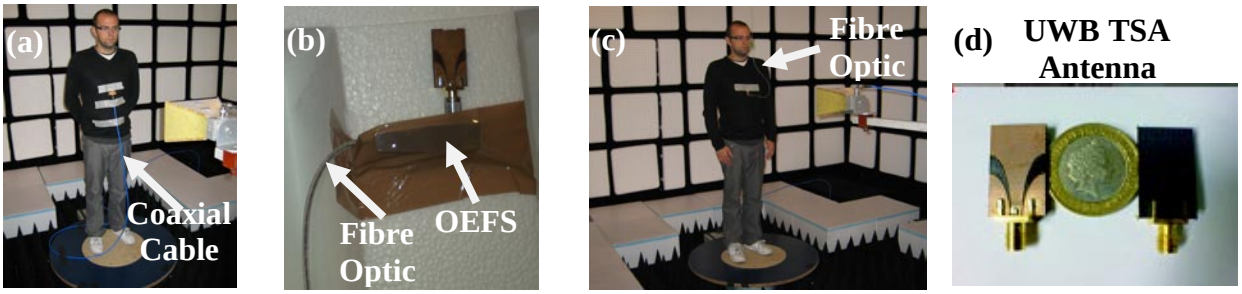

Figures 11: (a) A typical measurement set-up using a coaxial cable for body-worn antennas; (b) freespace fibre optic measurement set-up (close up of antenna taped to underside of foam block); (c) on-body fibre optic measurement set up at the NPL's SMART range facility; and (d) the proposed UWB TSA antenna placed next to a British two-pound coin.

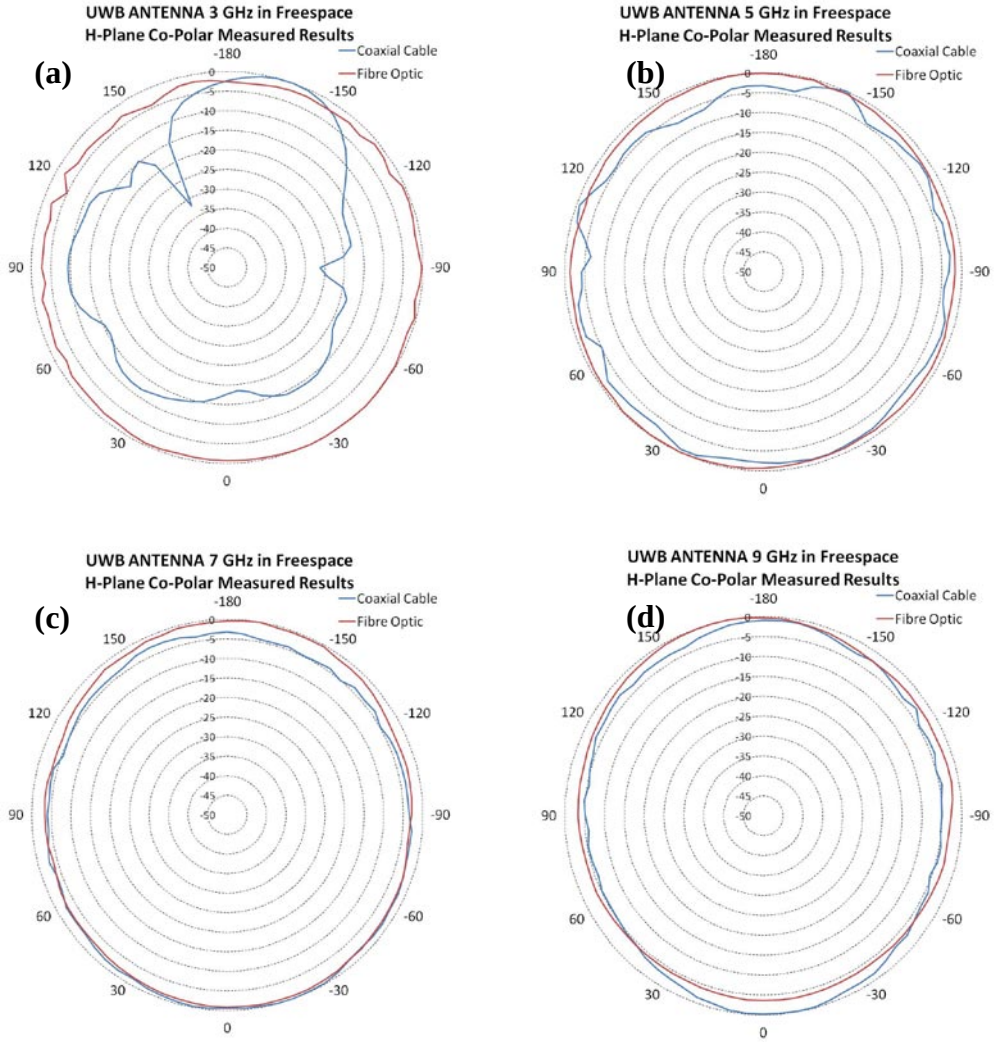

Figures 12 (a-d): Measured H-Plane (azimuth) radiation patterns in **freespace** at: 3 GHz, 5 GHz, 7 GHz and 9 GHz and comparison between coaxial cable and fibre optic set-up. Clearly at 3 GHz the pattern with coaxial is significantly distorted however the use of the fibre optic gives an excellent result.

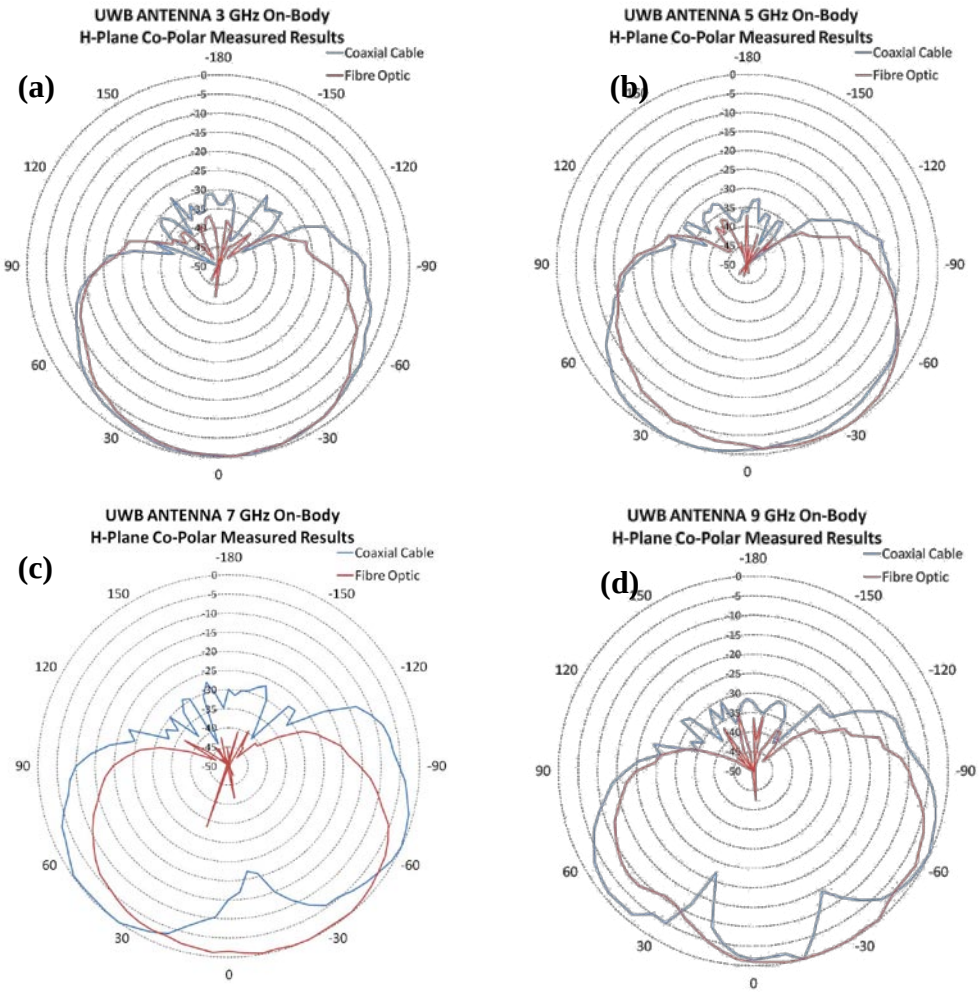

Figures 13 (a-d): Measured H-Plane (azimuth) radiation patterns **on-body** at 3 GHz, 5 GHz, 7 GHz and 9 GHz and comparison between coaxial cable and fibre optic set-up. It is evident that the higher frequency measurements (at 5 GHz and above) the pattern with coaxial is significantly distorted however the use of the fibre optic gives an excellent wide beamwidth which is in excellent agreement with simulated results.

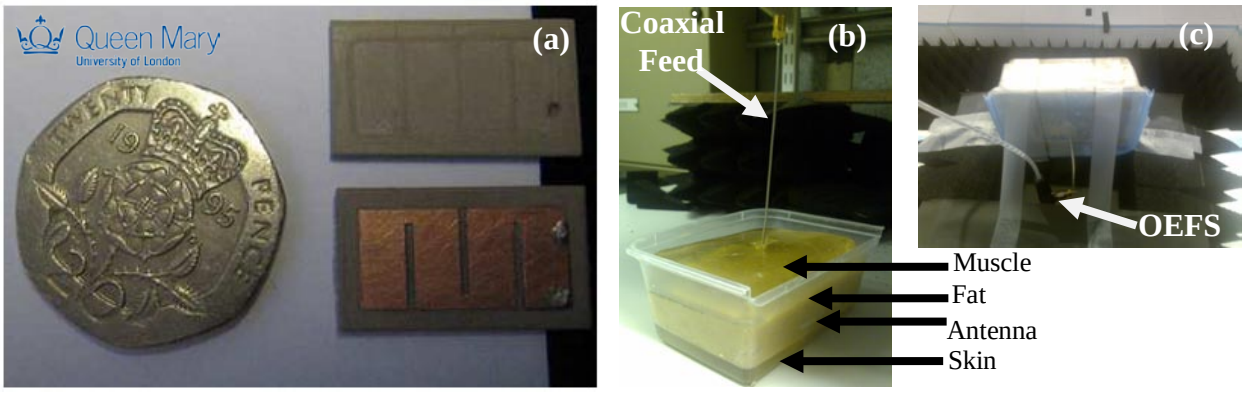

Figures 14: (a) photo of the fabricated implantable RFID antenna (substrate with radiating element dismounted from the superstrate) on Rogers R03010 (^{2}r= 10.2, h = 1.27mm) placed next to a British 20 pence coin; (b) photo of the fabricated 3-layered phantom and the coaxial feeder that allows the flow of common mode currents; (c) Photo of the measurement set-up using the OEFS transducer, fibre-optic system.

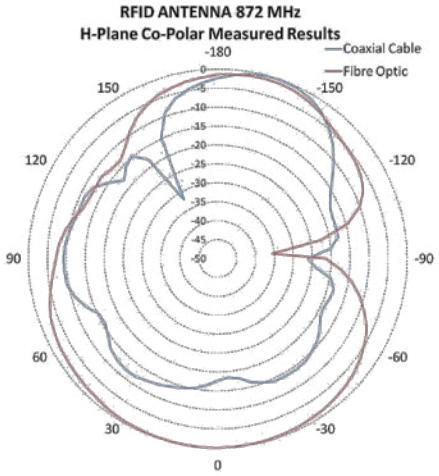

Figure 15. Measured H-Plane (azimuth) radiation patterns of **implantable RFID antenna** at 872 MHz and comparison between coaxial cable and fibre optic set-up. The result verifies that the use of the fibre optic system can decrease measurement errors caused by flowing common mode currents by as much as 18 dB (0 deg angle).

Conclusions

An investigation has been carried out at 2 GHz in the NPL SMART chamber on the invasiveness of antenna supports on the radiated field of electrically small antennas. This is a glimpse of the intended frequency range of 900 MHz to 10.3 GHz that covers most wireless applications including the UWB bands. When a resonant dipole antenna was mounted clear above the mast, or with its null directed to the mast, the effect on the H-plane pattern was estimated to be within 0.25 dB; also an excellent E-plane pattern was obtained. However when the dipole was mounted at the end of the Orbit foam platform with it's mainlobe in the direction of the mast, the pattern was obscured by up to 2.5 dB when the mast intervened between the dipole and the source antenna, a configuration to be avoided where possible.

The measurement of a PIFA antenna without a balun showed dramatically the improvement in the pattern measured over a sphere when the coaxial cable was substituted by the RF-optical transducer. The miniature size of this transducer is key to being able to measure small antennas non-invasively. This was well illustrated by measurements of body mounted and implantable antennas in the frequency range 3 GHz to 10 GHz.

Acknowledgements

This work was funded in part by the Physical Programme 2006 – 2009 of the National Measurement System (NMS) Policy Unit of the UK Department for Innovation, Universities and Skills (DIUS). Seikoh-giken lent an OEFS-CII-10GHz optical electric field sensor system; masayuki.kimura@seikoh-giken.co.jp.

References

[1] P.S. Hall and Y. Hao (Editors), "Antennas and Propagation for Body-Centric Wireless Communications", Artech House, 2006.

[2] T. H. Loh, M. Alexander, F. Widmer, P. Miller, D. Knight, "Validation of a New Small-Antenna Radiated Testing Range", 3rd European Conference on Antenna and Propagation (EuCAP 2009), Berlin, Mar. 2009.

[3] A. Alomainy, A. Sani, J. Santas, A. Rahman, and Y. Hao, "Transient characteristics of wearable antennas and radio propagation channels for ultra wideband body-centric wireless communications," in press for IEEE Transactions in Antenna and Propagation, 2009, awaiting publication.

[4] Y. Hao and R. Foster, "Wireless body sensor networks for health-monitoring applications," Physiol. Meas., vol. 29, pp. R27–R56, Nov. 2008.